Fast Power Control for VSCs to Enhance the Synchronization Stability in Ultra-Weak Grids

Yang, Dongsheng; Wang, Xiongfei; Blaabjerg, Frede

Published in:
Proceedings of the IEEE Power & Energy Society General Meeting (PESGM 2018)

DOI (link to publication from Publisher):
10.1109/PESGM.2018.8586308

Publication date:
2018

Document Version
Accepted author manuscript, peer reviewed version

Fast Power Control for VSCs to Enhance the Synchronization Stability in Ultra-Weak Grids

Dongsheng Yang, Xiongfei Wang, Frede Blaabjerg
Department of Energy Technology, Aalborg University.
Pontoppidanstraede 101, Aalborg, 9220, Denmark
doy@et.aau.dk, xwa@et.aau.dk, fbl@et.aau.dk

***Abstract*—In order to effectively transmit the renewable power to the remote load center, more and more utility-scale renewable generation systems have to be operated under the ultra weak gird condition, i.e., the Short-Circuit Ratio (SCR) of power transmission lines impedance is close to 1. As a result, the steady-state operating point of load angle is close to the stability limit 90°. Even a small grid disturbance can result in small-signal power instability, and trigger off the whole renewable generation system, resulting in catastrophic cascading failure in the power system. In this paper, a novel fast power control method is proposed for the interfacing grid-connected Voltage-Source Converters (VSCs). With this method, the power control bandwidth can be increased far beyond the fundamental frequency, which provides superior dynamic power control performance. More importantly, the load angle can be safely limited within the stable region against the grid disturbance by quickly reducing the input power. As a result, the synchronization stability of VSC is greatly improved. The control method is verified by both analytical models and experimental results.**

***Index Terms*—Synchronization stability, Fast Power Control, Voltage Source Converter (VSC), Ultra-weak grid condition.**

I. INTRODUCTION

Benefiting from the significant technical advances of renewable generation sources and power electronics, the penetration level of renewable energy in the power system keeps on increasing [1]. In order to alleviate the cost of upgrading the whole grid infrastructure, more and more utility-scale renewable generation systems and the corresponding transmission systems are connected to the ultra-weak gird, i.e., the Short-Circuit Ratio (SCR) of power transmission lines is close to 1.0 [2]-[3]. However, dynamic interactions between the interfacing grid-connected Voltage-Source Converters(VSCs) and the ultra weak grid tend to bring in various of resonance and stability issues, challenging stable operations of modern power systems.

The dominated control scheme for the grid-connected VSCs is the vector control, which regulates the instantaneous active power and reactive power through the inner current control loop. In order to synchronize with the grid, a Phase-Locked Loop (PLL) is used to obtain the accurate phase angle of the voltage at the point of common coupling (PCC). However, PLL tends to make the VSC behave like a negative resistor [4]-[5], which tends to trigger resonances [6]-[7].

To eliminate the negative impact of PLL, the power synchronization control is proposed which operates the grid-connected VSCs in a similar way as a synchronous machine [8]. In principle, it is a voltage-controlled scheme under normal operation, which regulates the active power by adjusting the load angle of the terminal voltage, while regulates its reactive power by varying its voltage magnitude. Similarly, many algorithms of Virtual Synchronous Generators (VSGs) are also proposed to enhance the stability of the power system dominated by power electronics [9]-[11]. However, under the ultra-weak grid condition with SCR close to 1.0, the load angle, i.e., the phase difference between the terminal voltage of VSC and the grid voltage, is very close to stability limit 90° [12]. Even a small grid disturbance can bring in synchronization instability, and trigger off the whole renewable generation system, resulting in catastrophic cascading failure in the power system. As a result, the transferred active power of VSC in the steady-state should be intentionally reduced in reality to ensure enough transient load angle margin [8].

In this paper, a novel cross-modulation power control method is proposed for the grid-connected VSC with the voltage-controlled scheme. By cross-modulating the amplitude and angle of the terminal voltage, the power control bandwidth can be increased far beyond the fundamental frequency, which provides superior dynamic power control performance. More importantly, the load angle can be safely limited within the stable region against the grid disturbance. As a result, the synchronization stability of VSC is greatly improved. The control method is verified by both analytical models and experimental results.

II. MODELING OF THE POWER CONTROL LOOPS

The typical voltage-controlled scheme of the grid-connected VSC is shown in Fig. 1. The grid impedance is modeled by an inductor L_g and a resistor r_g. The output active and reactive power are firstly calculated using the terminal voltage $\boldsymbol{e}_{\alpha\beta}$ and injected grid current $\boldsymbol{i}_{\alpha\beta}$ in the $\alpha\beta$ frame. Then, the active power error is fed into the power regulator $G_P(s)$, and its output is used to adjust the frequency ω and thereby the phase angle of the terminal voltage. Similarly, the reactive power error is fed into the power regulator $G_Q(s)$ and its output is used to adjust the magnitude of the terminal voltage vector $\boldsymbol{e}_{\alpha\beta}$.

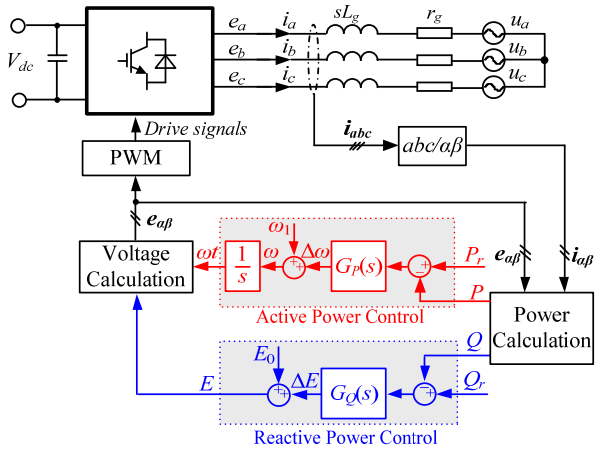

Fig.1 Voltage-controlled scheme of grid-connected VSC

According to the definition of the instantaneous power [13], the output complex power can be derived as:

$$\begin{aligned}\boldsymbol{S}(t) &= \boldsymbol{e}_{\alpha\beta}(t)\cdot\boldsymbol{i}_{\alpha\beta}(t)^* \\ &= \boldsymbol{e}_{dq}(t)e^{j\omega_1 t}\cdot\left(\boldsymbol{i}_{dq}(t)e^{j\omega_1 t}\right)^* = \boldsymbol{e}_{dq}(t)\cdot\boldsymbol{i}_{dq}(t)^*\end{aligned} \tag{1}$$

where $\boldsymbol{e}_{dq}$ and $\boldsymbol{i}_{dq}$ are the terminal voltage and grid current vectors in the dq frame, respectively. ω_1 is the fundamental frequency of the grid voltage. The superscript asterisk * donates conjugation operator.

To obtain the small signal model of the power control, the small signal perturbation is performed, i.e.,

$$\begin{aligned}&\boldsymbol{S}_0+\Delta\boldsymbol{S}(t)=\left(\boldsymbol{E}_{dq0}+\Delta\boldsymbol{e}_{dq}(t)\right)\cdot\left(\boldsymbol{I}_{dq0}+\Delta\boldsymbol{i}_{dq}(t)\right)^* \\ &\Rightarrow \Delta\boldsymbol{S}(t)=\boldsymbol{E}_{dq0}\Delta\boldsymbol{i}_{dq}^*(t)+\boldsymbol{I}_{dq0}^*\Delta\boldsymbol{e}_{dq}(t)\end{aligned} \tag{2}$$

where $\boldsymbol{E}_{dq0}$ and $\boldsymbol{I}_{dq0}$ are the steady-state value of the terminal voltage and grid current vectors, respectively, while the $\Delta\boldsymbol{e}_{dq}$ and $\Delta\boldsymbol{i}_{dq}$ are the corresponding small signal perturbations. Applying the Laplace transformation to (2), yields

$$\Delta\boldsymbol{S}(s)=\boldsymbol{E}_{dq0}\Delta\boldsymbol{i}_{dq}^*(s)+\boldsymbol{I}_{dq0}^*\Delta\boldsymbol{e}_{dq}(s) \tag{3}$$

Similarly, applying the small signal perturbation to the voltage vector $\boldsymbol{e}_{dq}$, yields

$$\begin{aligned}\boldsymbol{e}_{dq}(t)&=\left(E_0+\Delta E(t)\right)e^{j(\theta_0+\Delta\theta(t))} \\ &\approx \underbrace{E_0e^{j\theta_0}}_{\boldsymbol{E}_{dq0}}+\underbrace{\Delta E(t)e^{j\theta_0}+jE_0e^{j\theta_0}\Delta\theta(t)}_{\Delta\boldsymbol{e}_{dq}(t)}\end{aligned} \tag{4}$$

where E_0 and θ_0 are the steady-state value of magnitude and the load angle of the terminal volage and grid current vectors, while the ΔE and $\Delta\ \theta$ are corresponding small signal perturbations. Therefore, the expressions of the $\boldsymbol{E}_{dq0}$ and $\Delta\boldsymbol{e}_{dq}$ in the frequency domain can be derived as

$$\boldsymbol{E}_{dq0}=E_0e^{j\theta_0},\ \Delta\boldsymbol{e}_{dq}(s)=\Delta E(s)e^{j\theta_0}+jE_0e^{j\theta_0}\Delta\theta(s) \tag{5}$$

Likewise, the expressions of $\boldsymbol{I}_{dq0}$ and $\Delta\boldsymbol{i}_{dq0}$ can also be derived as

$$\boldsymbol{I}_{dq0}=\frac{\boldsymbol{E}_{dq0}-\boldsymbol{U}_{dq0}}{\boldsymbol{Z}_{gdq0}},\ \Delta\boldsymbol{i}_{dq}(s)=\frac{\Delta\boldsymbol{e}_{dq}(s)}{\boldsymbol{Z}_{gdq}(s)} \tag{6}$$

where the expressions of steady-state grid voltage $\boldsymbol{U}_{dq0}$, grid impedances $\boldsymbol{Z}_{dq}(s)$ and $\boldsymbol{Z}_{dq0}$ are given by:

$$\boldsymbol{U}_{dq0}=U_0e^{j0}=U_0 \tag{7}$$

$$\begin{aligned}&\boldsymbol{Z}_{gdq}(s)=sL_g+r_g+j\omega_1L_g, \\ &\boldsymbol{Z}_{gdq0}=\boldsymbol{Z}_{gdq}(s)\big|_{s=0}=r_g+j\omega_1L_g\end{aligned} \tag{8}$$

For high-power high voltage applications, r_g can be neglected. So substituting (5)-(8) into (3), yields

$$\begin{aligned}\Delta\boldsymbol{S}(s)=&\underbrace{\left(\frac{\omega_1L_gE_0}{\left(sL_g\right)^2+\left(\omega_1L_g\right)^2}-\frac{E_0-U_0\cos\theta_0}{\omega_1L_g}\right)E_0}_{G_{\theta P}(s)}\cdot\Delta\theta(s) \\ &+\underbrace{\left(\frac{sL_gE_0}{\left(sL_g\right)^2+\left(\omega_1L_g\right)^2}+\frac{U_0\sin\theta_0}{\omega_1L_g}\right)}_{G_{EP}(s)}\cdot\Delta E(s) \\ &+j\underbrace{\left(\frac{U_0\sin\theta_0}{\omega_1L_g}-\frac{sL_gE_0}{\left(sL_g\right)^2+\left(\omega_1L_g\right)^2}\right)E_0}_{G_{\theta Q}(s)}\cdot\Delta\theta(s) \\ &+j\underbrace{\left(\frac{\omega_1L_gE_0}{\left(sL_g\right)^2+\left(\omega_1L_g\right)^2}+\frac{E_0-U_0\cos\theta_0}{\omega_1L_g}\right)}_{G_{EQ}(s)}\cdot\Delta E(s)\end{aligned} \tag{9}$$

III. Limitation of Stability and Control Bandwidth

The strength of the grid can be depicted by the SCR, of which the expression is given by:

$$SCR=\frac{P_{SC}}{P_n}=\frac{E_0^2/(\omega_1L_g)}{P_n} \tag{10}$$

where P_n is the rated power of VSC, and P_{SC} is the short-circuit power at the PCC.

In steady-state, the output active power of VSC is well known [8], which is expressed as

$$P=\frac{EU}{\omega_1L_g}\sin\theta \tag{11}$$

Therefore, the steady-state load angle θ_0 can be given by:

$$\theta_0=\arcsin\frac{P_0\omega_1L_g}{E_0U_0} \tag{12}$$

According to (10) and (12), the steady-state load angle θ_0 with respective to SCR can be derived as

$$\theta_0=\arcsin\frac{P_0\omega_1L_g}{E_0U_0}=\arcsin\left(\frac{P_0}{P_n}\frac{E_0}{U_0}\frac{1}{SCR}\right) \tag{13}$$

Therefore, under the ultra weak grid condition with SCR close to 1.0, the steady-state load angle is very close to 90° if the steady-state output power P_0 is close to its rated value P_n.

Substituting s=0 into (9), the steady-state gain of $G_{\theta P}(s)$ can be obtained as

$$G_{\theta P}(0)=\left(\frac{\omega_1 L_g E_0}{\left(\omega_1 L_g\right)^2}-\frac{E_0-U_0\cos\theta_0}{\omega_1 L_g}\right)E_0=\frac{U_0 E_0\cos\theta_0}{\omega_1 L_g} \quad (14)$$

As a result, the steady-state gain of $G_{\theta P}(s)$ is close to zero under the ultra weak grid condition. More seriously, a small voltage dip of U_0 can make the steady-state load angle θ_0 drift over 90°, which will change the active power control loop from the negative feedback control into the positive feedback control, resulting in synchronization instability.

Another issue is that a pair of conjugate poles is found for all the power control transfer functions, which will generate a −180° phase jump at the fundamental frequency ω_1 and impose a great limitation on the power control bandwidth.

According to Fig.2, the active power loop and reactive power loop are coupled with each other due $G_{\theta Q}(s)$ and $G_{EP}(s)$. Moreover, all $G_{\theta P}(s)$, $G_{EQ}(s)$, $G_{\theta Q}(s)$ and $G_{EP}(s)$ contain a pair of conjugate poles, which can be expressed as:

$$s_{1,2}=-r_g/L_g\pm j\omega_n \quad (15)$$

When the passive damping in the grid impedance is weak, i.e., $R/(L\omega_n)$ ratio is low, the poles will move closer to the imaginary axis. As a result, the oscillation can be potentially triggered near the synchronous frequency ω_1, namely synchronous frequency resonance (SFR). Fig. 2 gives the frequency responses of $G_{\theta P}(s)$, $G_{EQ}(s)$, $G_{\theta Q}(s)$ and $G_{EP}(s)$ when $R/(L\omega_n)$=1%. There are resonance peaks and −180° phase jump at the synchronous frequency (50Hz), which make it difficult to increase the control bandwidth of power loops above the synchronous frequency.

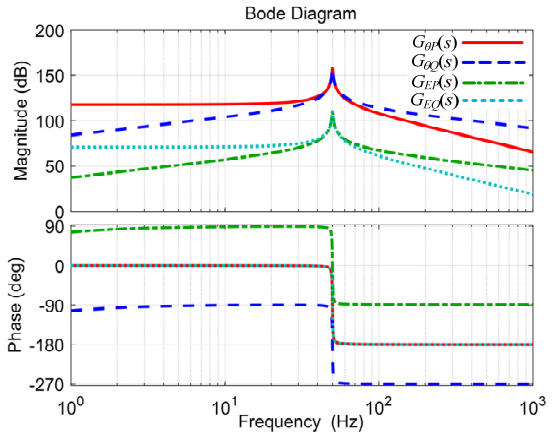

Fig. 2 Frequency responses of the control plant for power loops.

IV. Fast Power Control by Cross-Modulation

To solve the problems mentioned above, the cross-modulation power control method is proposed in this paper, as shown in Fig. 4. in principle, the cross-modulation is to regulate the active/reactive power by adjusting both the phase angle and the magnitude of the VSC output voltage, rather than just one of them. And the cross-modulation functions $G_{\theta E}(s)$ and $G_{E\theta}(s)$ are given by:

$$G_{\theta E}(s)=\frac{E_0}{\omega_1}s \quad (16)$$

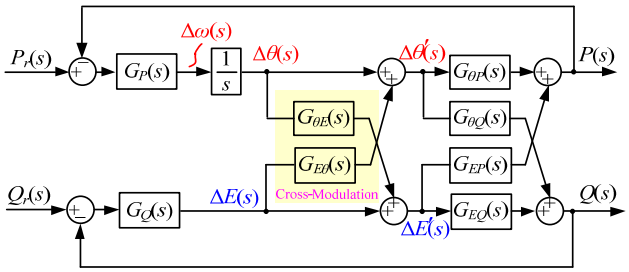

Fig. 3 Control scheme of the cross-modulation power control

$$G_{E\theta}(s)=-\frac{1}{E_0\omega_1}s \quad (17)$$

According to Fig 3, the equivalent control plant of power loops with cross-modulation power control can be derived as:

$$G'_{\theta P}(s)=G_{\theta P}(s)+G_{\theta E}(s)\cdot G_{EP}(s)=\frac{E_0U_0\cos\theta_0+E_0U_0\sin\theta_0\cdot s/\omega_1}{\omega_1 L_g} \quad (18)$$

$$G'_{\theta Q}(s)=G_{\theta Q}(s)+G_{\theta E}(s)\cdot G_{EQ}(s)=\frac{E_0U_0\sin\theta_0+\left(E_0^2-E_0U_0\cos\theta_0\right)\cdot s/\omega_1}{\omega_1 L_g} \quad (19)$$

$$G'_{EP}(s)=G_{EP}(s)+G_{E\theta}(s)\cdot G_{\theta P}(s)=\frac{U_0\sin\theta_0+\left(E_0-U_0\cos\theta_0\right)\cdot s/\omega_1}{\omega_1 L_g} \quad (20)$$

$$G'_{EQ}(s)=G_{EQ}(s)+G_{E\theta}(s)\cdot G_{\theta Q}(s)=\frac{2E_0-U_0\cos\theta_0-U_0\sin\theta_0\cdot s/\omega_1}{\omega_1 L_g} \quad (21)$$

As seen, compared with the control plants presented in (9), the conjugate poles in the denominator are eliminated by the proposed cross-modulation control. Therefore, the control bandwidth of the power control loops can be greatly improved.

V. Experimental Verification

Down-scaled experimental setup is built to verify the analytical results and the effectiveness of the proposed method. To emulate ultra-weak grid condition, a series inductor is connected with the regenerative grid simulator Chroma 61845. The VSC is implemented by Danfoss FC103P11KT 11 and the control algorithms are programmed in the dSPACE1007. The circuit parameters are shown in Table I, where the grid voltage is intentionally reduced to create the ultra grid condition with SCR = 1.0 for the worst case.

In this paper, the PI controller is used for active power control, while the proportion droop controller is used for the reactive power control. Moreover, the low pass filter is used to filter out the high-frequency power fluctuations. So the

expression of the active power controller $G_P(s)$ and reactive power controller $G_Q(s)$ can be given by

$$G_P(s) = \left(K_p + \frac{K_i}{s}\right)\frac{\omega_L}{s+\omega_L} \tag{22}$$

$$G_q(s) = D_q \frac{\omega_L}{s+\omega_L} \tag{23}$$

The detailed control parameters are shown in Table II.

Take the active power control loop as the example, when P_0 = 0.95 p.u. and SCR=1.0, the "active resistor" R_v has to be implemented [8] to damp the resonance peak at the fundamental frequency 50Hz if the cross-modulation power control is not used, as the solid-line shown in Fig. 4. Even though, −180° phase jump at the synchronous frequency (50Hz) makes it difficult to further improve the dynamic performance of the active power control. When the cross-modulation power control is employed, the resonance peak at the synchronous frequency is removed, thus the control bandwidth can be greatly improved, as the dashed line shown in Fig. 4.

Fig. 5 shows the dynamic waveforms when the active power reference changes between 0.9 p.u. and 0.95 p.u, where e_a and i_a are the terminal voltage and output current of the grid-connected VSC, respectively. The actual active power experiences a long-time transient without using cross-modulation power control, as shown in Fig. 5(a). While this transient is eliminated when the cross-modulation power control is employed, and the active power follows the reference in a very fast and smooth way, as shown in Fig. 5(b). Therefore, the proposed method is effective to improve the system dynamic performance.

Fig. 6 shows the dynamic waveforms when the 1Hz grid frequency disturbance occurs. Similarly, the proposed power control method shows stronger disturbance-rejection ability as shown in Fig 6.(b) compared with the conventional method that shown in Fig. 6(a).

Fig. 7 shows the dynamic waveforms when the 0.1 p.u. grid sag occurs. As seen, due to the fast power dynamic response of the proposed method, the load angle can be kept in the stable region by limiting the current through active power reference, as shown in Fig. 7 (b). However, the load angle drifts over 90° under such severe grid disturbance for the conventional method and lose of synchronization occurs, as shown in Fig. 7(a).

Table I. Main circuit parameters of tested VSC system

Parameters	Value
Grid voltage U_0 (L-L RMS)	60 V (1 p.u.)
Rated Active Power P_n	1 kW (1 p.u.)
fundamental frequency f_1	50 Hz
Switching frequency f_s	10 kHz
Grid inductor L_g (SCR = 1)	11.5 mH (1 p.u.)

Table II. Control parameters of the power controllers

Parameters	w/o cross-modulation	with cross-modulation
K_p	0.12	0.38
K_i	4.2	1000
R_v	0.25 p.u.	–
D_q	0.05 U_0/P_n	0.05 U_0/P_n
ω_L	500Hz*2π	500Hz*2π

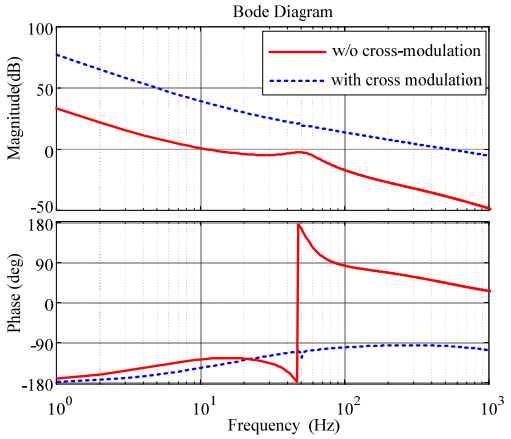

Fig. 4 Bode diagram of active power loop gains

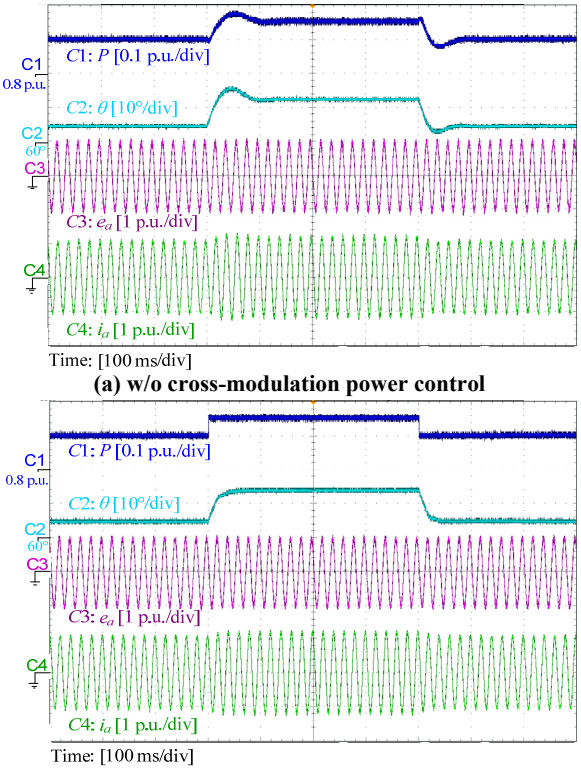

(a) w/o cross-modulation power control

(b) with cross-modulation power control

Fig. 5 Dynamic waveforms with a step change of active power reference between 0.9 p.u. to 0.95 p.u.

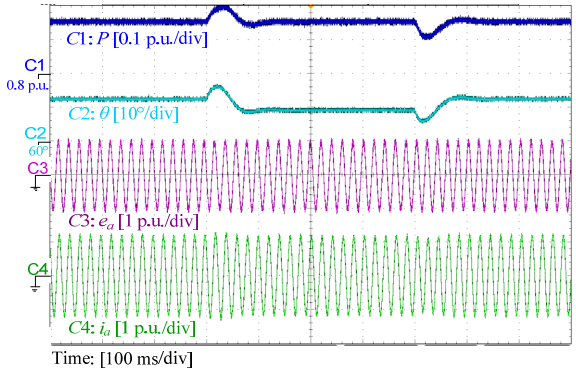

(a) w/o cross-modulation power control

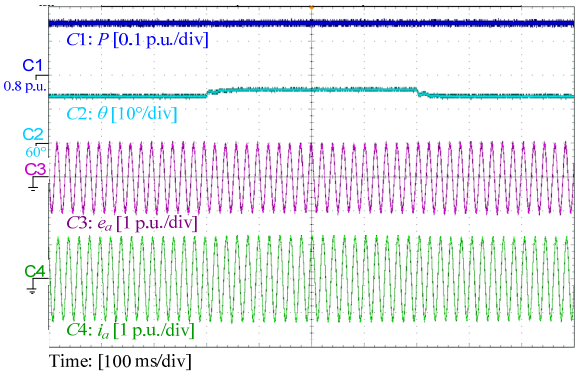

(b) with cross-modulation power control

Fig. 6 Dynamic waveforms with 1Hz grid frequency disturbance

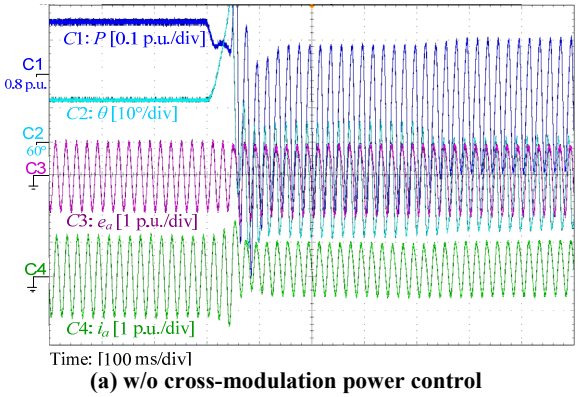

(a) w/o cross-modulation power control

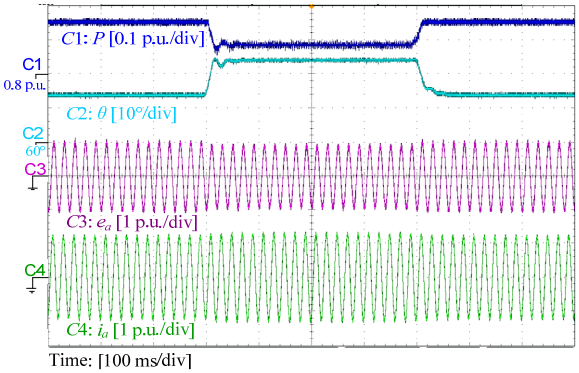

(b) with cross-modulation power control

Fig. 7 Dynamic waveforms with 0.1 p.u. voltage dip.

CONCLUSIONS

A novel cross-modulation power control method is proposed in this paper for the grid-connected VSC with the voltage-controlled scheme. By cross-modulating the amplitude and angle of the terminal voltage, the power control bandwidth can be increased far beyond the fundamental frequency, which provides superior dynamic power control performance. More importantly, the load angle can be safely limited within the stable region against the grid disturbance.

REFERENCES

[1] F. Blaabjerg, Y. Yang, D. Yang, and X Wang, "Distributed Power-Generation Systems and Protection," *Proc. IEEE*, 2017, 105 (7): 1311–1331.

[2] J. Zhou and A. Gole, "VSC transmission limitations imposed by AC system strength and AC impedance characteristics," in *Proc. 10th IET International Conference on AC and DC Power Transmission (ACDC)*, pp. 1–6, 2012.

[3] D. Yang, X. Wang, and F. Liu, K. Xin, Y. Liu, F. Blaabjerg, "Adaptive reactive power control of PV power plants for improved power transfer capability under ultra-weak grid conditions," *IEEE Trans. Smart Grid*, 2018, in press.

[4] L. Harnefors, M. Bongiornos, and S. Lundberg, "Input-admittance calculation and shaping for controlled voltage-source converters," *IEEE Trans. Ind. Electron.*, vol. 54, no.6 , pp. 3323–3334, 2007.

[5] T. Messo, J. Jokipii, A. Makinen, and T. Suntio, "Modeling the grid synchronization induced negative-resistor-like behavior in the output impedance of a three-phase photovoltaic inverter," in *Proc. IEEE Fourth Intl. Symp. Power Electron. for Distributed Generations System*, pp. 1–8, 2013.

[6] W. Bo, D. Dong, D. Boroyevich, R. Burgos, P. Mattavelli, and S. Zhiyu, "Impedance-based analysis of grid-synchronization stability for three-phase paralleled converters," *IEEE Trans. Power Electron.*, vol 31, no. 1, pp. 26–38, 2016.

[7] X. Wang, L. Harnefors, and F. Blaabjerg, "A unified impedance model of grid-connected voltage-source converters," *IEEE Trans. Power Electron.,* in press.

[8] L. Zhang, L. Harnefors, and H.-P. Nee, "Power-synchronization control of grid-connected voltage-source converters," *IEEE Trans. Power Syst.*, vol. 25, no. 2, pp. 809–820, 2010.

[9] Q.-C. Zhong and G. Weiss. "Synchronverters: Inverters that mimic synchronous generators, " *IEEE Trans. Ind. Electron*, volume 58, no. 4, pp. 1259–1267, 2011.

[10] T. Loix. "Participation of inverter-connected distributed energy resources in grid voltage control," PhD Dissertation, Leuven: Katholieke Universiteit Leuven, 2011.

[11] H. Wu, X. Ruan, D. Yang, X. Chen, W. Zhao, Z. Lv, Q. Zhong, "Small-signal modeling and parameters design for virtual synchronous generators," *IEEE Trans. Ind. Electron.,* vol 63, no. 7, pp. 4292–4303, 2016.

[12] A. Egea-Alvarez, S. Fekriasl, F. Hassan, and O. Gomis-Bellmunt, "Advanced vector control for voltage source converters connected to weak grids," *IEEE Trans. Power Syst.*, vol. 30, no. 6, pp. 3072–3081, 2015.

[13] H. Akagi, E. Watanabe, and M. Aredes. *Instantaneous Power Theory and Applications to Power Conditioning*. New Jersey: IEEE Press, 2007.